

R²-VOS: Robust Referring Video Object Segmentation via Relational Cycle Consistency

Xiang Li¹, Jinglu Wang², Xiaohao Xu³, Xiao Li², Yan Lu², Bhiksha Raj¹

¹Carnegie Mellon University, ²Microsoft Research Asia,

³Huazhong University of Science and Technology,
<https://lxa9867.github.io/works/rrvos>.

Abstract

Referring video object segmentation (R-VOS) aims to segment the object masks in a video given a referring linguistic expression to the object. It is a recently introduced task attracting growing research attention. However, all existing works make a strong assumption: The object depicted by the expression must exist in the video, namely, the expression and video must have an object-level semantic consensus. This is often violated in real-world applications where an expression can be queried to false videos, and existing methods always fail in such false queries due to abusing the assumption. In this work, we emphasize that studying semantic consensus is necessary to improve the robustness of R-VOS. Accordingly, we pose an extended task from R-VOS without the semantic consensus assumption, named Robust R-VOS (R²-VOS). The R²-VOS task is essentially related to the joint modeling of the primary R-VOS task and its dual problem (text reconstruction). We embrace the observation that the embedding spaces have relational consistency through the cycle of text-video-text transformation, which connects the primary and dual problems. We leverage the cycle consistency to discriminate the semantic consensus, thus advancing the primary task. Parallel optimization of the primary and dual problems are enabled by introducing an early grounding medium. A new evaluation dataset, R²-Youtube-VOS, is collected to measure the robustness of R-VOS models against unpaired videos and expressions. Extensive experiments demonstrate that our method not only identifies negative pairs of unrelated expressions and videos, but also improves the segmentation accuracy for positive pairs with a superior disambiguating ability. Our model achieves the state-of-the-art performance on Ref-DAVIS17, Ref-Youtube-VOS, and the novel R²-Youtube-VOS dataset.

1 Introduction

Referring video object segmentation (R-VOS) aims to segment a referred object in a video sequence given a linguistic expression. R-VOS has witnessed growing interest thanks to its promising potential in human-computer interaction applications such as video editing and augmented reality. Unlike other video segmentation tasks [42, 34, 33, 43] that only rely on visual cues, R-VOS [10] pairs a target video with a linguistic expression referring to an object.

Previous works [1, 41] tackle the R-VOS problem with a strong assumption that the referred object exists in the video, i.e., there is an object-level semantic consensus between the expression and the video. However, this assumption does not always hold in practice. As shown in Figure 1, we notice a severe false-alarm problem experienced by previous methods when the semantic consensus does not exist, which may prevent those methods from being useful in various applications that cannot provide accurate vision-language pairs. We argue that the current R-VOS task is not completely defined with the assumption that the referred object always exists in the video.

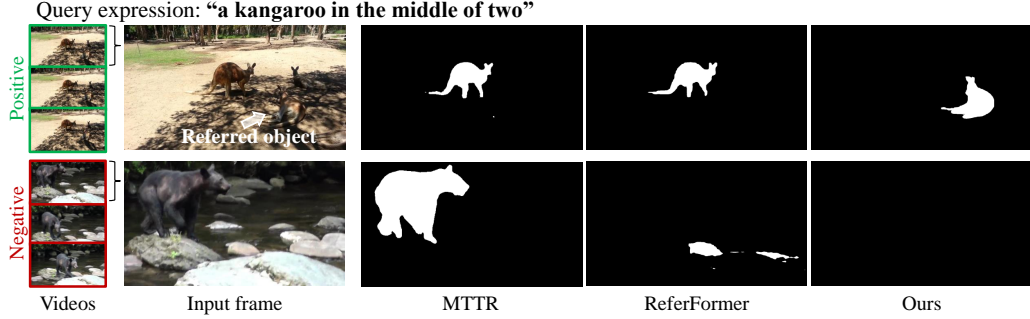


Figure 1: Illustration of the new R^2 -VOS task. A linguistic expression is given to query a set of videos without the semantic consensus assumption. Videos containing the referred object by the expression are **positive**, otherwise **negative**. Unlike the previous R-VOS setting that assumes all target videos are positive to the query expression, the new R^2 -VOS task is required to discriminate positive and negative text-video pairs, and further segment object masks for all frames in positive videos or treat entire negative videos as backgrounds. Compared to the previous state-of-the-art R-VOS methods, MTTR [1] and ReferFormer [41], our method not only discriminates negative videos better but also shows a superior disambiguating ability between visually similar objects in positive videos.

Even when semantic consensus exists in the given video-language pairs, it is still challenging to locate the correct object in the video due to the multimodal nature of the R-VOS task. Recently, MTTR [1] employs a multimodal transformer encoder to learn a joint representation of the linguistic expression and video, and then obtains the referred object by ranking all objects in the video. ReferFormer [41] follows the image-level method, ReTR [14], to adopt the linguistic expression as a query to the transformer decoder to avoid redundant ranking of all objects. However, these latest methods suffer from semantic misalignment of the segmented object and the linguistic expression, even with sophisticated components employed. As shown in Figure 1, the segmented objects by MTTR and ReferFormer are often not the object referred to by the linguistic expression.

In this paper, we seek to investigate the semantic alignment problem between visual and linguistic modalities in referring video segmentation. We extend the current task definition of R-VOS [10] to accept both paired and unpaired video and language inputs. This new task, which we term Robust R-VOS (R^2 -VOS), overcomes the current limitation of the R-VOS task by additionally considering the semantic alignment of input video to referring expression. We reveal that this task is essentially related to two problems that are interrelated [27]: the R-VOS problem as the **primary** problem of segmenting mask sequences from videos with referring texts, and its **dual** problem of reconstructing text expressions from videos with object masks. By linking the primary and dual problems, we introduce a text-video-text cycle and a corresponding relational consistency constraint, which can enforce the semantic consensus between the text query and segmented mask to improve the primary task. In practice, naively conducting cyclic training of the text-video-text cycle will lead to a two-stage regime and significantly increasing costs. We address this problem by incorporating an early grounding scheme, serving as a medium, to efficiently model the two tasks in a parallel manner. In addition, we discriminate the semantic misalignment between the video and text by assessing the cycle consistency between the original and reconstructed texts, thus alleviating the false-alarm problem. Our contributions can be summarized as:

- We notice a severe false-alarm problem faced by previous R-VOS methods with unpaired inputs. To investigate the robustness of current referring segmentation models, we introduce the R^2 -VOS task that accepts unpaired video and text as inputs.
- We propose a pipeline that jointly optimizes the primary referring segmentation and dual expression reconstruction task and introduces a relational cycle consistency constraint to enhance the semantic alignment between visual and textual modalities.
- Our method surpasses previous state-of-the-art methods on Ref-Youtube-VOS, Ref-DAVIS, and R^2 -Youtube-VOS dataset in terms of both performance and speed.

2 Related Works

Vision and language representation learning. For vision-language representation learning, visual-semantic embedding (VSE) [6] and its improved versions [30, 13, 28, 3] have been proposed to facilitate multimodal tasks, e.g., image-text matching. Recent works [21, 26, 3] introduce cross-modal attention layers and achieve superior improvement. KAC Net [2] leverages knowledge-aided consistency constraints to enhance semantic alignment for weakly supervised phrase grounding. A structure-preserving constraint [39] is proposed to preserve some intra-modal properties when learning vision-language representation for image-text retrieval.

Referring video object segmentation. R-VOS is a novel task that aims to segment an object across frames given a linguistic description. URVOS [36] is the first unified R-VOS framework with a cross-modal attention and a memory attention module, which largely improves R-VOS performance. ClawCraneNet [16] leverages cross-modal attention to bridge the semantic correlation between textual and visual modalities. ReferFormer [41] and MTTR [1] are two latest works that utilize transformers to decode or fuse multimodal features. ReferFormer [41] employs a linguistic prior to the transformer decoder to focus on the referred object. MTTR [1] leverages a multimodal transformer encoder to fuse linguistic and visual features. Different from other vision-language tasks, e.g., image-text retrieval [20, 22, 29] and video question answering [12, 37], R-VOS needs to construct object-level multimodal semantic consensus in a dense visual representation.

3 R²-VOS

3.1 Task Definition

We introduce a novel task, robust referring video segmentation (R²-VOS), which aims to predict mask sequences $\{M_o\}$ for an unconstrained video set $\{V\}$ given a language expression E_o of an object o . Different from the previous R-VOS setup, the queried video V is not required to contain the referred object by expression E_o . We define a video V and an expression E_o to have **semantic consensus** if the object o appears in V , and the video is **positive** with respect to E_o , otherwise it is **negative**. The R²-VOS task is extended to discriminate positive and negative videos, and predict masks M_o of object o for positive videos and treat all frames in the negative videos as background.

3.2 Problem Analysis

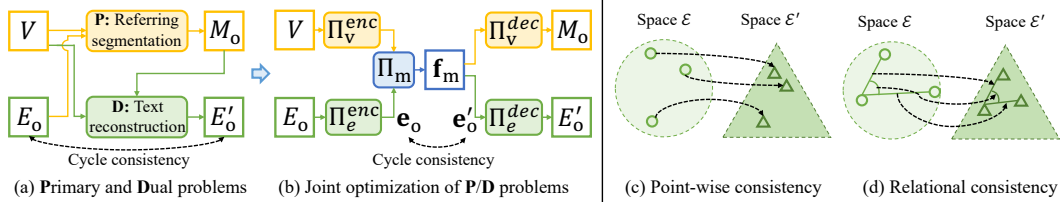


Figure 2: Problem analysis. (a) R²-VOS introduces the **Primary** problem of referring segmentation and the **Dual** problem of text reconstruction for positive videos. The **P/D** problems are connected in a cycle path from original expression E_o to reconstructed expression E'_o . (b) The cycle consistency between the original and reconstructed embeddings (e_o and e'_o) can benefit to optimize the **P** problem. We enable the joint optimization for cycle consistency with a cross-modal medium f_m defined between all single-modal operations (i.e., Π_v^{enc} , Π_e^{enc} , Π_v^{dec} and Π_e^{dec}). (c) Point-wise consistency is not suitable in R²-VOS because the mapping between \mathcal{E} and \mathcal{E}' are not necessarily bijective because an object can be referred to by various textual expressions. (d) Instead, we apply a relational consistency to preserve distances and angles.

Primary and dual problems for R²-VOS. The referring segmentation can be formulated as the maximum *a posteriori* estimation problem of $p(M_o|V, E_o)$. By applying the Bayes rule, we obtain:

$$p(M_o|V, E_o) \sim p(E_o|V, M_o)p(M_o|V) \quad (1)$$

As the prior $p(M_o|V)$ is not affected by the expression E_o , we consider maximizing $p(E_o|V, M_o)$ as a dual problem of the referring segmentation (primary problem), which is to reconstruct the text expression given the video and object masks. We note that for negative videos, $p(E_o|V, M_o)$ is

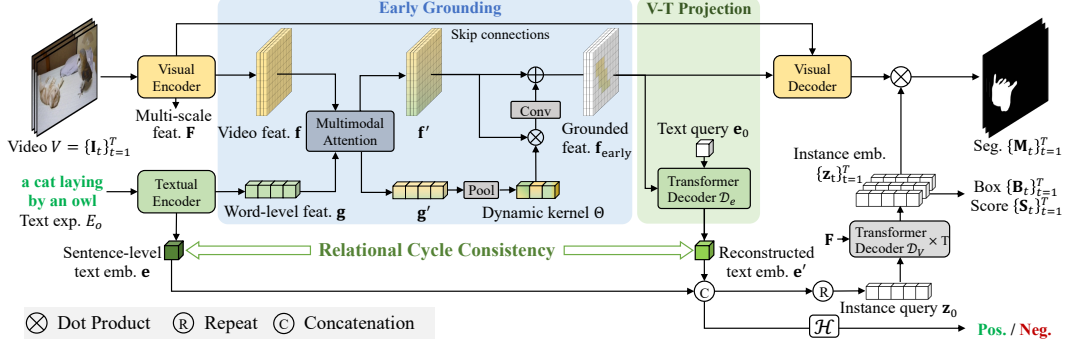


Figure 3: Overview of the proposed model. Given a video clip $V = \{I_t\}_{t=1}^T$ and a textual expression E_o referring object o , we first extract video feature and text feature separately, then fuse them in the early grounding module to obtain the visual representation f_{early} of the referred object o . Then we project f_{early} to a textual space to be e' and add the relational cycle constraint with the original text embedding e . The final segmentation is obtained by dynamic convolutions with video features from the visual decoder and dynamic weights from the fused text embeddings. The semantic consensus of input pairs is discriminated to be positive or negative by assessing the consistency between e and e' .

undefined because the mask M_o is empty. Thus, we only investigate the dual problem for positive videos. The primary problem and the dual problem can be connected in a cycle path, i.e., from the original expression E_o to the reconstructed expression E'_o through positive video queries, as shown in Figure 2 (a). We believe that the cycle constraint benefits to optimize the primary problem by enhancing the semantic consensus.

In practice, we study the cycle consistency between the original textual embedding space \mathcal{E} and the transformed textual embedding space \mathcal{E}' induced by positive videos. By definition, the path from the original text embedding e_o to the reconstructed text embedding e'_o is modulated with **cross-modal** interactions between video and text. Thus, to link the primary and dual problem and enable the joint optimization, we introduce a cross-modal medium f_m to convey information of both the input of the primary problem (V, E_o) and the dual problem (V, M_o) , as shown in Figure 2 (b). f_m is defined between the encoder and decoder stages of single-modal operations, i.e., $\Pi_v^{\text{enc}}, \Pi_e^{\text{enc}}, \Pi_v^{\text{dec}}, \Pi_e^{\text{dec}}$, to only focus on the multi-modal interaction.

Relational cycle consistency. A key observation for cycle consistency between \mathcal{E} and \mathcal{E}' is that the mapping between them is not necessarily bijective, as there could be multiple textual descriptions for the same object. Thus, naively adding point-wise consistency, i.e., $e_o = e'_o, \forall e_o \in \mathcal{E}$ will collapse the feature space to a sub-optimal solution. Instead, we take inspiration from relational knowledge distillation [31], and introduce relational cycle consistency for \mathcal{E} and \mathcal{E}' . The relational cycle consistency is to preserve the structure of the feature space rather than exact point-wise consistency, as illustrated in Figure 2 (c) and (d). Mathematically, the structure-preserving property is defined as isometric and conformal constraints to preserve pair-wise distance and angles for $e \in \mathcal{E}$ and $e' \in \mathcal{E}'$:

$$|e_1 - e_2| = |e'_1 - e'_2| \quad (2)$$

$$\angle(e_1, e_2, e_3) = \angle(e'_1, e'_2, e'_3), \quad (3)$$

where $|\cdot|$ and $\angle(\cdot)$ denote distance and angle metrics.

4 Method

In this section, we elaborate our R^2 -VOS framework with the relational consistency, which mainly consists of four parts: feature extraction, early grounding as a medium, video-text (V-T) projection for text reconstruction, and mask decoding for final segmentation, as shown in Figure 3. We first extract the video feature f , word-level text feature g , and sentence-level text embedding e . On the one hand, to model the primary segmentation problem of maximizing $p(M_o|V, E_o)$, we enable the multimodal interaction in the early grounding module to generate the grounded feature f_{early} . f_{early} coarsely locates the referred object o and filters out irrelevant features, which serves as a medium linking the primary segmentation and dual text reconstruction problem. The final mask M_o is obtained by dynamic convolution [4] on the decoded visual feature maps, with kernels learned from instance

embedding $\{z_t\}_{t=1}^T$. On the other hand, to model the dual text reconstruction problem of maximizing $p(E_o|V, M_o)$, we utilize the grounded video feature $\mathbf{f}_{\text{early}}$ as the alternative of V and M_o , since $\mathbf{f}_{\text{early}}$ conveys contextual video clues of object o . In this way, we enable the parallel optimization of the primary and dual problem by relating them to $\mathbf{f}_{\text{early}}$. Specifically, we employ a V-T projection module to project $\mathbf{f}_{\text{early}}$ onto a reconstructed text embedding \mathbf{e}' . We add relational constraint between \mathbf{e}' and \mathbf{e} to enforce the semantic alignment between the segmented mask and expression for positive videos. In addition, we introduce a semantic consensus discrimination head $\mathcal{H}(\mathbf{e}, \mathbf{e}')$ to assess the consistency between original and reconstructed text embeddings, discriminating the alignment of multimodal semantics and identifying negative videos.

4.1 Single-modal Feature Extraction

Visual encoder. Following previous methods [1, 41, 40], we build the visual encoder with a visual backbone and a deformable transformer encoder [46] on top of it. The extracted features from the backbone are flattened, projected to a lower dimension, added with positional encoding [9], and then fed into a deformable transformer encoder [46] similar to the previous method [41]. We denote the multi-scale output of the transformer encoder as \mathbf{F} and the low-resolution visual feature map from the backbone as \mathbf{f} , where $\mathbf{f} \in \mathbb{R}^{T \times C_v \times \frac{H}{32} \times \frac{W}{32}}$, C_v is the feature channel, T is the video length and H and W are the original image size.

Textual encoder. We leverage a pre-trained linguistic model RoBERTa [23] to map the input textual expression E_o to a textual embedding space. The textual encoder extracts a sequence of word-level text feature $\mathbf{g} \in \mathbb{R}^{C_e \times L}$ and a sentence-level text embedding $\mathbf{e} \in \mathbb{R}^{C_e \times 1}$, where C_e and L are the dimension of linguistic embedding space and the expression length respectively.

4.2 Early Grounding

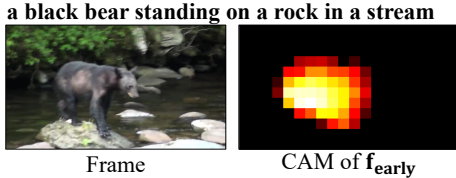


Figure 4: Visualization of channel activation map (CAM) of $\mathbf{f}_{\text{early}}$.

Figure 3, we first enable the multimodal interaction between video and text features, then apply the dynamic convolution with kernels learned from text feature to discriminate the object-level semantics. In particular, multi-head cross-attention (MCA) [38] is leveraged to conduct the multimodal interaction:

$$\mathbf{h}_f = \text{LN}(\text{MCA}(\mathbf{f}, \mathbf{g}) + \mathbf{f}) \quad \mathbf{f}' = \text{LN}(\text{FFN}(\mathbf{h}_f) + \mathbf{h}_f) \quad (4)$$

$$\mathbf{h}_g = \text{LN}(\text{MCA}(\mathbf{g}, \mathbf{f}) + \mathbf{g}) \quad \mathbf{g}' = \text{LN}(\text{FFN}(\mathbf{h}_g) + \mathbf{h}_g), \quad (5)$$

where $\text{MCA}(\mathbf{X}, \mathbf{Y}) = \text{Attention}(\mathbf{W}^Q \mathbf{X}, \mathbf{W}^K \mathbf{Y}, \mathbf{W}^V \mathbf{Y})$. \mathbf{W} represents learnable weight. LN and FFN denote layer normalization and feed-forward network respectively. The text feature \mathbf{g}' is further pooled to a fixed length, and followed by a fully-connected layer to form the dynamic kernels $\Theta = \{\theta_i\}_{i=1}^K$. K is the kernel number and $\theta_i \in \mathbb{R}^{C \times 1}$. The dynamic kernels are applied separately to video feature $\mathbf{f}' \in \mathbb{R}^{C \times THW}$ to form the $\mathbf{f}_{\text{early}} \in \mathbb{R}^{C \times THW}$

$$\mathbf{f}_{\text{early}} = \text{BN}(\varphi(\theta_1^T \mathbf{f}' \oplus \dots \oplus \theta_K^T \mathbf{f}') + \mathbf{f}'), \quad (6)$$

where \oplus is the concatenation in channel dimension and $\varphi(\cdot)$ is a convolution to reduce the feature dimension. BN denotes batch normalization.

4.3 Text Reconstruction

V-T projection. We leverage a transformer decoder \mathcal{D}_E as textual decoder to transform the visual representation of the referred object into the textual space. As shown in Figure 3, a learnable text query $\mathbf{e}_0 \in \mathbb{R}^{C_e \times 1}$ is employed to query the $\mathbf{f}_{\text{early}}$. The output of the transformer decoder is the reconstructed text embedding $\mathbf{e}' = \mathcal{D}_E(\mathbf{f}_{\text{early}}, \mathbf{e}_0) \in \mathbb{R}^{C_e \times 1}$.

4.4 Referring Segmentation

Mask segmentation. Similar to previous methods [41, 1, 8], we leverage deformable transformer decoders with dynamic convolution to segment the object masks. As shown in Figure 3, we first fuse the reconstructed text embedding \mathbf{e}' to text embedding \mathbf{e} . The fused text embedding \mathbf{e} is then repeated N times to form the instance query [40] $\mathbf{z}_0 \in \mathbb{R}^{C_q \times N}$, where C_q is the dimension of instance query and N is the instance query number. We then use $T \times$ deformable transformer decoders \mathcal{D}_V with shared weights to decode the instance embeddings $\mathbf{z}_t \in \mathbb{R}^{C_q \times N}$ for each frame, i.e., $\mathbf{z}_t = \mathcal{D}_V(\mathbf{F}_t, \mathbf{z}_0)$. \mathbf{F}_t is the multiscale visual feature from visual encoder at time t . A dynamic kernel \mathbf{w}_t is further learned from the instance embedding \mathbf{z}_t . The final feature map $\mathbf{f}_{\text{out},t} \in \mathbb{R}^{C \times H \times W}$ is obtained by fusing low-level features from the feature pyramid network [18] in the visual decoder. The mask prediction $\mathbf{M}_t \in \mathbb{R}^{N \times H \times W}$ can be computed by $\mathbf{M}_t = \mathbf{w}_t^T \mathbf{f}_{\text{out},t}$.

Auxiliary heads. We build a set of auxiliary heads to obtain the final object masks across frames. In particular, a box head, a scoring head and a semantic consensus discrimination head are leveraged to predict the bounding boxes $\mathbf{B}_t \in \mathbb{R}^{N \times 4}$, confidence scores $\mathbf{S}_t \in \mathbb{R}^{N \times 1}$ and the alignment degree of multimodal semantics $A \in \mathbb{R}$. The box and scoring head are two fully-connected layers upon the instance embedding \mathbf{e}_t . The semantic consensus discrimination head $\mathcal{H}(\mathbf{e}, \mathbf{e}')$ consists of two fully-connected layers upon the text embeddings $\mathbf{e} \oplus \mathbf{e}'$. Note that A represents the semantic alignment in the entire video rather a single frame, since the expression is a video-level description.

4.5 Loss Function

The loss function of our method can be boiled down to three parts:

$$\mathcal{L} = \lambda_{\text{text}} \mathcal{L}_{\text{text}} + \lambda_{\text{segm}} \mathcal{L}_{\text{segm}} + \lambda_{\text{align}} \mathcal{L}_{\text{align}}, \quad (7)$$

where $\mathcal{L}_{\text{text}}$, $\mathcal{L}_{\text{segm}}$, and $\mathcal{L}_{\text{align}}$ are losses for text reconstruction, referring segmentation and semantic consensus discrimination respectively. The $\mathcal{L}_{\text{align}}$ is simply a cross-entropy loss between the predicted alignment A and ground-truth \hat{A} . The other two terms are computed as follows:

Loss for text reconstruction. Given the text embedding \mathbf{e} and reconstructed text embedding \mathbf{e}' , we employ a relational constraint to impose the cycle consistency between \mathbf{e} and \mathbf{e}' . We calculate the loss by

$$\mathcal{L}_{\text{text}} = \mathbb{1}(\hat{A}) \cdot (\mathcal{L}_{\text{dist}} + \lambda_{\text{angle}} \mathcal{L}_{\text{angle}}), \quad (8)$$

where the indicator function $\mathbb{1}(\hat{A}) = 1$ if the alignment indicates the referred object exists in the video, otherwise 0, λ_{angle} is a hyperparameter balancing the distance loss $\mathcal{L}_{\text{dist}}$ and angle loss $\mathcal{L}_{\text{angle}}$. We elaborate these two losses according to the relational cycle consistency Equation 2. Let $\mathcal{X}^n = \{(x_1, \dots, x_n) | x_i \in \mathcal{X}\}$ denote a set of n -tuples, $\Phi^n = \{(\mathbf{x}, \mathbf{x}') | \mathbf{x} \in \mathcal{X}^n, \mathbf{x}' \in \mathcal{X}'^n\}$ denote a set of pairs consisting of two n -tuples of distinct elements from two different sets \mathcal{X} and \mathcal{X}' . Specifically, the distance-based and angle-based relations relate text embeddings of 2-tuple and 3-tuple respectively, i.e., $\Phi^2 = \{(\mathbf{x}, \mathbf{x}') | \mathbf{x} = (\mathbf{e}_i, \mathbf{e}_j), \mathbf{x}' = (\mathbf{e}'_i, \mathbf{e}'_j), i \neq j\}$ and $\Phi^3 = \{(\mathbf{x}, \mathbf{x}') | \mathbf{x} = (\mathbf{e}_i, \mathbf{e}_j, \mathbf{e}_k), \mathbf{x}' = (\mathbf{e}'_i, \mathbf{e}'_j, \mathbf{e}'_k), i \neq j \neq k\}$. Then the losses are given by:

$$\mathcal{L}_{\text{dist}} = \sum_{(\mathbf{x}, \mathbf{x}') \in \Phi^2} l_\delta(\phi_D(\mathbf{x}), \phi_D(\mathbf{x}')), \quad \phi_D(\mathbf{x}) = \frac{1}{\mu(\mathbf{x})} \|\mathbf{e}_i - \mathbf{e}_j\|_2, \quad (9)$$

$$\mathcal{L}_{\text{angle}} = \sum_{(\mathbf{x}, \mathbf{x}') \in \Phi^3} l_\delta(\phi_\angle(\mathbf{x}), \phi_\angle(\mathbf{x}')), \quad \phi_\angle(\mathbf{x}) = \cos \angle(\mathbf{e}_i, \mathbf{e}_j, \mathbf{e}_k), \quad (10)$$

where $\mu(\mathbf{x}) = \sum_{\mathbf{x}=(x_1, x_2) \in \mathcal{X}^2} \frac{\|x_1 - x_2\|_2}{|\mathcal{X}^2|}$ is the average distance function, and the Huber loss $l_\delta(x, x') = \frac{1}{2}(x - x')^2$ if $|x - x'| \leq 1$, otherwise $|x - x'| - \frac{1}{2}$.

Loss for referring segmentation. Given a set of predictions $\mathbf{y} = \{\mathbf{y}_i\}_{i=1}^N$ and ground-truth $\hat{\mathbf{y}}$, where $\mathbf{y}_i = \{\mathbf{B}_{i,t}, \mathbf{S}_{i,t}, \mathbf{M}_{i,t}\}_{t=1}^T$ and $\hat{\mathbf{y}} = \{\hat{\mathbf{B}}_t, \hat{\mathbf{S}}_t, \hat{\mathbf{M}}_t\}_{t=1}^T$, we search for an assignment $\sigma \in \mathcal{P}_N$ with the highest similarity where \mathcal{P}_N is a set of permutations of N elements ($\hat{\mathbf{y}}$ is padded with \emptyset). The similarity can be computed as

$$\mathcal{L}_{\text{match}}(\mathbf{y}_i, \hat{\mathbf{y}}) = \lambda_{\text{box}} \mathcal{L}_{\text{box}} + \lambda_{\text{conf}} \mathcal{L}_{\text{conf}} + \lambda_{\text{mask}} \mathcal{L}_{\text{mask}}, \quad (11)$$

where λ_{box} , λ_{conf} , and λ_{mask} are weights to balance losses. Following previous works [5, 40], we leverage a combination of Dice [15] and BCE loss as $\mathcal{L}_{\text{mask}}$, focal loss [19] as $\mathcal{L}_{\text{conf}}$, and GIoU

[35] and L1 loss as \mathcal{L}_{box} . The best assignment $\hat{\sigma}$ is solved by Hungarian algorithm [11]. Given the best assignment $\hat{\sigma}$, the segmentation loss between ground-truth and predictions is defined as $\mathcal{L}_{segm} = \mathbb{1}(\hat{A}) \cdot \mathcal{L}_{match}(\mathbf{y}, \hat{\mathbf{y}}_{\hat{\sigma}(i)})$.

4.6 Inference

During inference, we select the candidate with the highest confidence to predict the final masks:

$$\{\bar{\mathbf{M}}_t\}_{t=1}^T = \{\mathbb{1}(A) \cdot \mathbf{M}_{\bar{s},t}\}_{t=1}^T, \quad \bar{s} = \underset{i}{\operatorname{argmax}} \{\mathbf{S}_{i,1} + \dots + \mathbf{S}_{i,T}\}_{i=1}^N, \quad (12)$$

where $\{\bar{\mathbf{M}}_t\}_{t=1}^T$ is the masks of referred object. $\mathbf{S}_{i,t}$ and $\mathbf{M}_{i,t}$ represent the i -th candidate in \mathbf{S}_t and \mathbf{M}_t respectively. \bar{s} is the slot with the highest confidence to be the target object. We use $\mathbb{1}(A)$ to filter out predictions in negative videos to mitigate false alarm.

5 Experiment

5.1 Dataset and Metrics

Dataset. We conduct experiments on three datasets: Ref-Youtube-VOS, Ref-DAVIS and R²-Youtube-VOS. Ref-Youtube-VOS [36] is a large-scale benchmark that has 3,978 videos with about 15k language descriptions. There are 3,471 videos with 12,913 expressions in the training set and 507 videos with 2,096 expressions in the validation set. Ref-DAVIS-17 [10] contains 90 videos with 1,544 expressions, including 60 and 30 videos for training and validation respectively. R²-Youtube-VOS is our newly proposed evaluation dataset: it extends the Ref-Youtube-VOS validation set with each linguistic expression to query a positive video (the same one as Ref-Youtube-VOS) and a negative video. To make each video can be picked as a negative video, we randomly shuffle the original video set and constrain all negative text-video pair unrelated.

Metrics. We employ commonly-used region similarity \mathcal{J} and contour accuracy \mathcal{F} [34] for conventional Ref-Youtube-VOS and Ref-DAVIS-17 benchmarks. For the proposed R²-Youtube-VOS task, we additionally introduce a new metric $\mathcal{R} = 1 - \frac{\sum_{M \in \mathcal{M}_{neg}} |M|}{\sum_{M \in \mathcal{M}_{pos}} |M|}$ to evaluate the degree of object false alarm in negative videos, where \mathcal{M}_{neg} and \mathcal{M}_{pos} are the sets containing segmented masks in negative and positive videos respectively. $|M|$ denotes the foreground area of mask M . The total foreground area of positive videos $\sum_{M \in \mathcal{M}_{pos}} |M|$ serves as a normalization term. Ideally, a model should treat all the negative videos as backgrounds with $\mathcal{R} = 1$.

5.2 Implementation Details

Following previous methods [5, 41], our model is first pre-trained on Ref-COCO+/g dataset [45, 27] and then finetuned on Ref-Youtube-VOS. The model is trained for 6 epochs with a learning rate multiplier of 0.1 at the 3rd and the 5th epoch. The initial learning rate is 1e-4 and a learning rate multiplier of 0.5 is applied to the backbone. We adopt a batchsize of 8 and an AdamW [25] optimizer with weight decay 1×10^{-4} . Following convention [41, 1], the evaluation on Ref-DAVIS directly uses models trained on Ref-Youtube-VOS without re-training. All images are cropped to have the longest side of 640 pixels and the shortest side of 360 pixels during training and evaluation. The window size is set to 5. Our method is implemented with PyTorch [32].

5.3 Main Results

We compare our method with state-of-the-art R-VOS methods on Ref-Youtube-VOS and Ref-DAVIS-17 in Table 1, and R²-VOS task in Table 2.

Comparison on Ref-Youtube-VOS. In Table 1, we first compare our method on Ref-Youtube-VOS. For results of ResNet [7] backbone, our method achieves 57.3 $\mathcal{J}\&\mathcal{F}$ which outperforms the latest method ReferFormer [41] by 1.7 $\mathcal{J}\&\mathcal{F}$. In addition, our method runs at 30 FPS compared to 22 FPS of state-of-the-art ReferFormer (FPS is measured using single NVIDIA P40 with $batchsize = 1$). For results of Swin-Transformer [24, 24] backbones, our method achieves 60.2 $\mathcal{J}\&\mathcal{F}$ and 61.3 $\mathcal{J}\&\mathcal{F}$ with Swin-Tiny and Video-Swin-Tiny backbones respectively, which outperforms ReferFormer [41] and MTTR [1] by a clear margin.

Method	Backbone	Ref-Youtube-VOS			Ref-DAVIS-17		
		$\mathcal{J} \& \mathcal{F}$	\mathcal{J}	\mathcal{F}	$\mathcal{J} \& \mathcal{F}$	\mathcal{J}	\mathcal{F}
Spatial Visual Backbone							
CMSA [44]	ResNet-50	34.9	33.3	36.5	34.7	32.2	37.2
CMSA + RNN [44]	ResNet-50	36.4	34.8	38.1	40.2	36.9	43.5
URVOS [36]	ResNet-50	47.2	45.3	49.2	51.5	47.3	56.0
PMINet [5]	ResNet-101	53.0	51.5	54.5	-	-	-
CITD [17]	ResNet-101	56.4	54.8	58.1	-	-	-
ReferFormer* [41]	ResNet-50	55.6	54.8	56.5	58.5	55.8	61.3
Ours	ResNet-50	57.3	56.1	58.4	59.7	57.2	62.4
ReferFormer* [41]	Swin-T	58.7	57.6	59.9	-	-	-
Ours	Swin-T	60.2	58.9	61.5	-	-	-
Spatio-temporal Visual Backbone							
MTTR* [1]	Video-Swin-T	55.3	54.0	56.6	-	-	-
ReferFormer* [41]	Video-Swin-T	59.4	58.0	60.9	-	-	-
Ours	Video-Swin-T	61.3	59.6	63.1	-	-	-

Table 1: **Comparison to state-of-the-art R-VOS methods on Ref-Youtube-VOS and Ref-DAVIS-17 val set.** * indicates results imported from preprints.

Method	Backbone	$\mathcal{J} \& \mathcal{F} \& \mathcal{R}$	\mathcal{J}	\mathcal{F}	\mathcal{R}
ReferFormer* [41]	ResNet-50	47.3	54.8	56.5	30.6
Ours	ResNet-50	69.5	55.9	58.4	94.1
MTTR* [1]	Video-Swin-T	40.0	55.9	58.1	5.9
ReferFormer* [41]	Video-Swin-T	49.1	58.0	60.9	28.5
Ours	Video-Swin-T	72.8	59.6	63.1	95.7

Table 2: **Comparison to state-of-the-art R-VOS methods on R²-Youtube-VOS.**

Comparison on Ref-DAVIS-17. Our method achieves 59.7 $\mathcal{J} \& \mathcal{F}$ on Ref-DAVIS-17 dataset, which outperforms ReferFormer by 1.2 $\mathcal{J} \& \mathcal{F}$.

Comparison on R²-VOS. As shown in Table 2, the state-of-the-art R-VOS methods, ReferFormer and MTTR suffer from a low \mathcal{R} metric which measures the false-alarm problem when the semantic consensus of the input text-video pair does not hold. Compared to the severe false alarm of previous R-VOS methods, our model successfully mitigates the false alarm of the model, thanks to the proposed multimodal cycle consistency constraint and semantic consensus discrimination head.

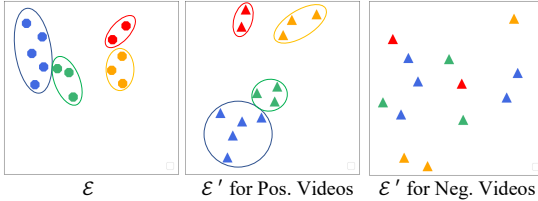


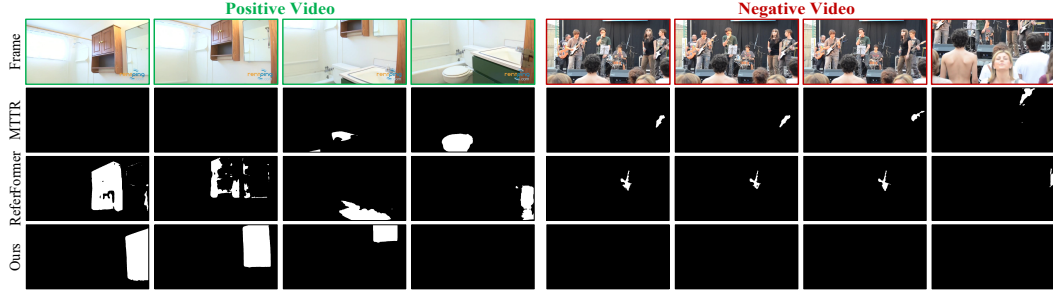
Figure 5: Visualization of text embedding spaces. Dots represent original text embeddings in \mathcal{E} , and triangles represent reconstructed ones in \mathcal{E}' induced by positive and negative videos respectively. Elements in the same color belong to the same object. Note that an object can have multiple text descriptions. The structure of \mathcal{E}' is well preserved from \mathcal{E} for positive videos (ellipses bound embeddings of same objects), while it is not preserved for negative videos.

As shown in Figure 5, we notice that, for embeddings of positive videos, they preserve relative relations well, while for negative videos, the reconstructed embeddings have a random pattern in the space.

Qualitative results. We compare the qualitative results of our method against state-of-the-art methods in Figure 6 on R²-VOS. For **positive videos**: The result indicates that our method predicts accurate and temporal-consistent results, while ReferFormer [41] and MTTR [1] fail to locate the correct object. For **negative videos**: Both ReferFormer and MTTR suffer from a severe false-alarm problem when the referred object does not exist in the video. In contrast, with multi-modal cycle constraint and consensus discrimination, our method successfully filters out negative videos and mitigates the false alarm. To further explore how the consensus discrimination works, we visualize the text embedding and

5.4 Ablation Study

Module effectiveness. To investigate the effectiveness of different components in our method, we conduct experiments with the ResNet-50 backbone on Ref-Youtube-VOS validation set. We build a transformer-based baseline model and equip our proposed components step-by-step. As shown in Table 3, the baseline model achieves 52.4 $\mathcal{J} \& \mathcal{F}$. After employing the early grounding module, the performance boosts to 55.5 $\mathcal{J} \& \mathcal{F}$ and the cycle-consistency constraint brings another 1.4 $\mathcal{J} \& \mathcal{F}$ gain. Since the reconstructed text embedding is generated with visual features injected, we consider it can



Expression: **the mirror in the bathroom is to the right of the wood cabinet**

Figure 6: Qualitative comparison to the state-of-the-art R-VOS method on the R^2 -VOS task.

Components	$\mathcal{J}\&\mathcal{F}$	\mathcal{J}	\mathcal{F}
Baseline	52.4	51.9	52.8
+EG	55.5+3.1	54.4	56.5
+CC	56.9+4.5	55.7	58.1
+FT	57.3+4.9	56.1	58.4

Table 3: **Impact of different components in our method.** EG: Early grounding, CC: Consistency constraint, FT: Fusing text embeddings.

Query Number	$\mathcal{J}\&\mathcal{F}$	\mathcal{J}	\mathcal{F}
1	54.9	54.2	55.6
5	57.3	56.1	58.4
9	57.0	56.8	57.2

Table 5: **Impact of the query number.**

Constraint	$\mathcal{J}\&\mathcal{F}$	\mathcal{J}	\mathcal{F}
None	55.5	54.4	56.5
PW	54.4-1.1	53.3	55.5
RA	56.7+1.2	55.5	57.9
RD	56.4+0.9	55.2	57.6
RD+RA	56.9+1.4	55.7	58.1

Table 4: **Impact of the cycle consistency constraint.** PW: Point-wise. RA: Relational angle. RD: Relational distance.

Window Size	$\mathcal{J}\&\mathcal{F}$	\mathcal{J}	\mathcal{F}
1	53.5	53.0	54.0
3	56.8	56.5	57.1
5	57.3	56.1	58.4

Table 6: **Impact of the window size.**

encode some visual information, thus augmenting the original text embedding. By using the fused text embedding as instance query, we achieve our best performance of 57.3 $\mathcal{J}\&\mathcal{F}$.

Consistency constraint. We conduct experiments to ablate the influence of cycle-consistency constraints. As shown in Table 4, utilizing point-wise consistency constraint will lead to a performance drop compared to the setting without cycle constraint. We consider the point-wise constraint may force an injective mapping from the textual domain to the visual domain. However, the mapping can be a many-to-one function for R-VOS, i.e., each object corresponds to multiple textual descriptions. In addition, since the early grounding leverages the text feature to locate the referred object, if we use the direct point-wise constraint to form reconstructed text embedding, it will encourage the network to memorize the text feature in the $\mathbf{f}_{\text{early}}$ and result in a collapse for text reconstruction. Table 4 shows that sole relational angle constraint can bring 1.2 $\mathcal{J}\&\mathcal{F}$ gain, and it can be slightly improved with 1.4 $\mathcal{J}\&\mathcal{F}$ gain by jointly using relational angle and distance constraint.

Instance query number. Although only one referral is involved for each frame in R-VOS task, to help the network optimization, we employ more than one instance query to each video. Table 5 indicates that a query number of 5 brings the best result.

Frame number. Since R-VOS gives a text that describes an object over a period of time, temporal information is vital to segment accurate and temporal-consistent results. We ablate on the best window size of input videos during training. As shown in Table 6, we notice that the performance improves as the window size increases and a window size of 5 brings the best result of 57.3 $\mathcal{J}\&\mathcal{F}$.

6 Conclusion

In this paper, we investigate the semantic misalignment problem in R-VOS task. A pipeline jointly models the referring segmentation and text reconstruction problem, equipped with a relational cycle consistency constraint, is introduced to discriminate and enhance the semantic consensus between visual and textual modalities. To evaluate the model robustness, we extend the R-VOS task to accept unpaired inputs and collect a corresponding R^2 -Youtube-VOS dataset. We observe a severe false-alarm problem suffered from previous methods on R^2 -Youtube-VOS while ours accurately discriminates unpaired inputs and segments high-quality masks for paired inputs. Our method achieves state-of-the-art performance on Ref-DAVIS17, Ref-Youtube-VOS, and R^2 -VOS dataset. We believe that, with unpaired inputs, R^2 -VOS is a more general setting of referring video segmentation, which can shed light on a new direction to investigate the robustness of referring segmentation.

References

- [1] Adam Botach, Evgenii Zheltonozhskii, and Chaim Baskin. End-to-end referring video object segmentation with multimodal transformers. *arXiv preprint arXiv:2111.14821*, 2021.
- [2] Kan Chen, Jiyang Gao, and Ram Nevatia. Knowledge aided consistency for weakly supervised phrase grounding. In *Proceedings of the IEEE Conference on Computer Vision and Pattern Recognition*, pages 4042–4050, 2018.
- [3] Yen-Chun Chen, Linjie Li, Licheng Yu, Ahmed El Kholy, Faisal Ahmed, Zhe Gan, Yu Cheng, and Jingjing Liu. Uniter: Universal image-text representation learning. In *European conference on computer vision*, pages 104–120. Springer, 2020.
- [4] Yinpeng Chen, Xiyang Dai, Mengchen Liu, Dongdong Chen, Lu Yuan, and Zicheng Liu. Dynamic convolution: Attention over convolution kernels. In *Proceedings of the IEEE/CVF Conference on Computer Vision and Pattern Recognition*, pages 11030–11039, 2020.
- [5] Zihan Ding, Tianrui Hui, Shaofei Huang, Si Liu, Xuan Luo, Junshi Huang, and Xiaoming Wei. Progressive multimodal interaction network for referring video object segmentation. *The 3rd Large-scale Video Object Segmentation Challenge*, page 7, 2021.
- [6] Fartash Faghri, David J Fleet, Jamie Ryan Kiros, and Sanja Fidler. Vse++: Improving visual-semantic embeddings with hard negatives. *arXiv preprint arXiv:1707.05612*, 2017.
- [7] Kaiming He, Xiangyu Zhang, Shaoqing Ren, and Jian Sun. Deep residual learning for image recognition. In *Proceedings of the IEEE conference on computer vision and pattern recognition*, pages 770–778, 2016.
- [8] Aishwarya Kamath, Mannat Singh, Yann LeCun, Gabriel Synnaeve, Ishan Misra, and Nicolas Carion. Mdetr-modulated detection for end-to-end multi-modal understanding. In *Proceedings of the IEEE/CVF International Conference on Computer Vision*, pages 1780–1790, 2021.
- [9] Guolin Ke, Di He, and Tie-Yan Liu. Rethinking positional encoding in language pre-training. *arXiv preprint arXiv:2006.15595*, 2020.
- [10] Anna Khoreva, Anna Rohrbach, and Bernt Schiele. Video object segmentation with language referring expressions. In *Asian Conference on Computer Vision*, pages 123–141. Springer, 2018.
- [11] Harold W Kuhn. The hungarian method for the assignment problem. *Naval research logistics quarterly*, 2(1-2):83–97, 1955.
- [12] Jie Lei, Licheng Yu, Mohit Bansal, and Tamara L Berg. Tvqa: Localized, compositional video question answering. *arXiv preprint arXiv:1809.01696*, 2018.
- [13] Kunpeng Li, Yulun Zhang, Kai Li, Yuanyuan Li, and Yun Fu. Visual semantic reasoning for image-text matching. In *Proceedings of the IEEE/CVF International conference on computer vision*, pages 4654–4662, 2019.
- [14] Muchen Li and Leonid Sigal. Referring transformer: A one-step approach to multi-task visual grounding. *Advances in Neural Information Processing Systems*, 34, 2021.
- [15] Xiaoya Li, Xiaofei Sun, Yuxian Meng, Junjun Liang, Fei Wu, and Jiwei Li. Dice loss for data-imbalanced nlp tasks. *arXiv preprint arXiv:1911.02855*, 2019.
- [16] Chen Liang, Yu Wu, Yawei Luo, and Yi Yang. Clawcranenet: Leveraging object-level relation for text-based video segmentation. *arXiv preprint arXiv:2103.10702*, 2021.
- [17] Chen Liang, Yu Wu, Tianfei Zhou, Wenguan Wang, Zongxin Yang, Yunchao Wei, and Yi Yang. Rethinking cross-modal interaction from a top-down perspective for referring video object segmentation. *arXiv preprint arXiv:2106.01061*, 2021.
- [18] Tsung-Yi Lin, Piotr Dollár, Ross Girshick, Kaiming He, Bharath Hariharan, and Serge Belongie. Feature pyramid networks for object detection. In *Proceedings of the IEEE conference on computer vision and pattern recognition*, pages 2117–2125, 2017.
- [19] Tsung-Yi Lin, Priya Goyal, Ross Girshick, Kaiming He, and Piotr Dollár. Focal loss for dense object detection. In *Proceedings of the IEEE international conference on computer vision*, pages 2980–2988, 2017.
- [20] Tsung-Yi Lin, Michael Maire, Serge Belongie, James Hays, Pietro Perona, Deva Ramanan, Piotr Dollár, and C Lawrence Zitnick. Microsoft coco: Common objects in context. In *European conference on computer vision*, pages 740–755. Springer, 2014.

- [21] Fenglin Liu, Yuanxin Liu, Xuancheng Ren, Xiaodong He, and Xu Sun. Aligning visual regions and textual concepts for semantic-grounded image representations. *Advances in Neural Information Processing Systems*, 32, 2019.
- [22] Yang Liu, Samuel Albanie, Arsha Nagrani, and Andrew Zisserman. Use what you have: Video retrieval using representations from collaborative experts. *arXiv preprint arXiv:1907.13487*, 2019.
- [23] Yinhan Liu, Myle Ott, Naman Goyal, Jingfei Du, Mandar Joshi, Danqi Chen, Omer Levy, Mike Lewis, Luke Zettlemoyer, and Veselin Stoyanov. Roberta: A robustly optimized bert pretraining approach. *arXiv preprint arXiv:1907.11692*, 2019.
- [24] Ze Liu, Jia Ning, Yue Cao, Yixuan Wei, Zheng Zhang, Stephen Lin, and Han Hu. Video swin transformer. *arXiv preprint arXiv:2106.13230*, 2021.
- [25] Ilya Loshchilov and Frank Hutter. Decoupled weight decay regularization. *arXiv preprint arXiv:1711.05101*, 2017.
- [26] Jiasen Lu, Dhruv Batra, Devi Parikh, and Stefan Lee. Vilbert: Pretraining task-agnostic visiolinguistic representations for vision-and-language tasks. *Advances in neural information processing systems*, 32, 2019.
- [27] Junhua Mao, Jonathan Huang, Alexander Toshev, Oana Camburu, Alan L Yuille, and Kevin Murphy. Generation and comprehension of unambiguous object descriptions. In *Proceedings of the IEEE conference on computer vision and pattern recognition*, pages 11–20, 2016.
- [28] Nicola Messina, Giuseppe Amato, Andrea Esuli, Fabrizio Falchi, Claudio Gennaro, and Stéphane Marchand-Maillet. Fine-grained visual textual alignment for cross-modal retrieval using transformer encoders. *ACM Transactions on Multimedia Computing, Communications, and Applications (TOMM)*, 17(4):1–23, 2021.
- [29] Antoine Miech, Ivan Laptev, and Josef Sivic. Learning a text-video embedding from incomplete and heterogeneous data. *arXiv preprint arXiv:1804.02516*, 2018.
- [30] Hyeonseob Nam, Jung-Woo Ha, and Jeonghee Kim. Dual attention networks for multimodal reasoning and matching. In *Proceedings of the IEEE conference on computer vision and pattern recognition*, pages 299–307, 2017.
- [31] Wonpyo Park, Dongju Kim, Yan Lu, and Minsu Cho. Relational knowledge distillation. In *Proceedings of the IEEE/CVF Conference on Computer Vision and Pattern Recognition*, pages 3967–3976, 2019.
- [32] Adam Paszke, Sam Gross, Francisco Massa, Adam Lerer, James Bradbury, Gregory Chanan, Trevor Killeen, Zeming Lin, Natalia Gimelshein, Luca Antiga, et al. Pytorch: An imperative style, high-performance deep learning library. *arXiv preprint arXiv:1912.01703*, 2019.
- [33] Federico Perazzi, Jordi Pont-Tuset, Brian McWilliams, Luc Van Gool, Markus Gross, and Alexander Sorkine-Hornung. A benchmark dataset and evaluation methodology for video object segmentation. In *Proceedings of the IEEE conference on computer vision and pattern recognition*, pages 724–732, 2016.
- [34] Jordi Pont-Tuset, Federico Perazzi, Sergi Caelles, Pablo Arbeláez, Alex Sorkine-Hornung, and Luc Van Gool. The 2017 davis challenge on video object segmentation. *arXiv preprint arXiv:1704.00675*, 2017.
- [35] Hamid Rezatofighi, Nathan Tsoi, JunYoung Gwak, Amir Sadeghian, Ian Reid, and Silvio Savarese. Generalized intersection over union: A metric and a loss for bounding box regression. In *Proceedings of the IEEE/CVF Conference on Computer Vision and Pattern Recognition*, pages 658–666, 2019.
- [36] Seonguk Seo, Joon-Young Lee, and Bohyung Han. Urvos: Unified referring video object segmentation network with a large-scale benchmark. In *Computer Vision–ECCV 2020: 16th European Conference, Glasgow, UK, August 23–28, 2020, Proceedings, Part XV 16*, pages 208–223. Springer, 2020.
- [37] Xiaomeng Song, Yucheng Shi, Xin Chen, and Yahong Han. Explore multi-step reasoning in video question answering. In *Proceedings of the 26th ACM international conference on Multimedia*, pages 239–247, 2018.

- [38] Ashish Vaswani, Noam Shazeer, Niki Parmar, Jakob Uszkoreit, Llion Jones, Aidan N. Gomez, undefinedukasz Kaiser, and Illia Polosukhin. Attention is all you need. NIPS'17, page 6000–6010, Red Hook, NY, USA, 2017. Curran Associates Inc.
- [39] Liwei Wang, Yin Li, and Svetlana Lazebnik. Learning deep structure-preserving image-text embeddings. In *Proceedings of the IEEE conference on computer vision and pattern recognition*, pages 5005–5013, 2016.
- [40] Yuqing Wang, Zhaoliang Xu, Xinlong Wang, Chunhua Shen, Baoshan Cheng, Hao Shen, and Huaxia Xia. End-to-end video instance segmentation with transformers. In *Proceedings of the IEEE/CVF Conference on Computer Vision and Pattern Recognition*, pages 8741–8750, 2021.
- [41] Jiannan Wu, Yi Jiang, Peize Sun, Zehuan Yuan, and Ping Luo. Language as queries for referring video object segmentation. *arXiv preprint arXiv:2201.00487*, 2022.
- [42] Ning Xu, Linjie Yang, Yuchen Fan, Dingcheng Yue, Yuchen Liang, Jianchao Yang, and Thomas Huang. Youtube-vos: A large-scale video object segmentation benchmark. *arXiv preprint arXiv:1809.03327*, 2018.
- [43] Linjie Yang, Yuchen Fan, and Ning Xu. Video instance segmentation. In *Proceedings of the IEEE/CVF International Conference on Computer Vision*, pages 5188–5197, 2019.
- [44] Linwei Ye, Mrigank Rochan, Zhi Liu, and Yang Wang. Cross-modal self-attention network for referring image segmentation. In *Proceedings of the IEEE/CVF Conference on Computer Vision and Pattern Recognition*, pages 10502–10511, 2019.
- [45] Licheng Yu, Patrick Poirson, Shan Yang, Alexander C Berg, and Tamara L Berg. Modeling context in referring expressions. In *European Conference on Computer Vision*, pages 69–85. Springer, 2016.
- [46] Xizhou Zhu, Weijie Su, Lewei Lu, Bin Li, Xiaogang Wang, and Jifeng Dai. Deformable detr: Deformable transformers for end-to-end object detection. *arXiv preprint arXiv:2010.04159*, 2020.